Contents list available at CBIORE journal website

International Journal of Renewable Energy Development

Journal homepage: https://ijred.cbiore.id

Research Article

Integrated rural energy system planning based on POA and stage division under the background of economic development

Xinghua Guo*

Student Affairs Department, Nanyang Institute of Technology, Nanyang, 47300, China

Abstract. Driven by the global energy transition and the "dual carbon" goals, the planning of rural integrated energy systems faces complex challenges such as dispersed demands, insufficient utilization of renewable resources, weak infrastructure, and differences in economic development stages. To address these issues, this study proposes a dynamic planning framework that integrates the macroeconomic development stage classification and improves the multi-objective pelican optimization algorithm. The algorithm dynamically adjusts the target weights and constraint boundaries based on the macroeconomic development stage. The algorithm initializes the population using the Sobol sequence combined with weak Gaussian perturbation and introduces an adaptive dynamic factor embedded with stage information to jointly adjust the search step size. A two-stage stochastic programming model with the objective of minimizing the total annual equivalent cost and maximizing the annual net carbon reduction is constructed. Simulation examples using typical rural areas in northern China show that the proposed algorithm outperforms the comparison algorithms in terms of convergence and distribution of solution sets. The Pareto solution set distribution index is the best at 0.082. The average annual total cost of the optimization scheme is 14.856 million yuan, which is 2.5% to 4.9% lower than the comparison algorithm, and the annual net carbon reduction is 634.2 tons, with a comprehensive energy efficiency of 76.8%. This framework converts the a priori knowledge of macroeconomic stages into adaptive parameters of the algorithm, effectively connecting planning preferences with search strategies, and providing a dynamic decision-making tool that balances economy, low carbon, and reliability for rural areas at different development levels. It has theoretical and application value for the coordinated advancement of rural energy transition and rural revitalization.

Keywords: Integrated rural energy system; Pelican optimization algorithm; Multi-objective optimization; Stage division; Energy planning; Economic development

Received: 16th April 2026; Revised:15th July 2026; Accepted: 10th August 2026; Available online: 1st Sept 2026

1. Introduction

The deepening global energy transition and sustainable development agenda have positioned rural areas as a critical component of national economic and social progress. The clean, efficient, and intelligent transformation of rural energy systems has become a pivotal pathway toward achieving "dual carbon" targets and advancing the rural revitalization strategy. However, the planning of the Integrated Rural Energy System (IRES) faces unique complexities. Firstly, rural energy demands are highly dispersed and exhibit significant temporal and spatial heterogeneity: agricultural production (such as irrigation, harvesting), agricultural product processing and residential energy demands fluctuate greatly in different seasons and within the day, especially the heating demand in winter and the cooling demand in summer, which place higher demands on the system's peak regulation capacity (Shahrom *et al.* 2023). Secondly, rural renewable resources are diverse (such as biomass, solar energy, wind energy, etc.), but the development utilization rate is low and there is a lack of effective collaborative configuration means, resulting in both resource waste and energy shortage (Wu 2025). Thirdly, rural energy infrastructure is generally weak, with a lower grid coverage and power supply reliability than cities, and its development speed and quality are highly dependent on the stage and speed of regional economic growth (Qin *et al.* 2024).

Realizing the carbon neutrality goal in rural areas faces a series of unique challenges. On one hand, rural areas are important carbon emission sources, mainly from fossil fuel combustion, open-air incineration of agricultural waste, and improper treatment of livestock and poultry manure. On the other hand, rural areas also have significant potential for carbon reduction, through the development of biogas projects, the promotion of photovoltaic and wind power, and the implementation of electrification renovations, greenhouse gas emissions can be significantly reduced. However, due to the lack of effective policies and financial support, many low-carbon technologies are difficult to be applied in rural areas. Moreover, the slow progress of rural electrification is one of the main obstacles to the transformation of the energy system. The high cost of extending the power grid, low load density, and obvious seasonal electricity usage characteristics lead to low investment returns for power companies and long-term insufficiency in power supply reliability and power quality in rural areas (Irshad *et al.* 2024). In some remote rural areas, off-grid distributed energy systems may have technical feasibility, but their initial investment and maintenance costs are still unaffordable for local residents.

* Corresponding author
Email: guoxh18@outlook.com (X. Guo)

Meanwhile, multi-objective optimization methods have made significant progress in the field of energy system planning. Traditionally, deterministic algorithms such as linear programming and mixed integer programming have been widely used in energy system planning, but they have high computational complexity when dealing with high-dimensional, nonlinear, and multi-constraint problems, and are difficult to simultaneously optimize multiple conflicting goals such as economy, environment, and reliability (Wang *et al.* 2024). Heuristic algorithms such as genetic algorithms and particle swarm optimization can handle non-convex problems, but they still have deficiencies in convergence speed, local optimal avoidance, and uniformity of the Pareto frontier distribution (Jabari *et al.* 2024). In recent years, the Pelican Optimization Algorithm (POA) as an emerging meta-heuristic algorithm has shown superior performance due to its few parameters, simple structure, and the ability to balance global exploration and local exploitation (Chander *et al.* 2024). However, applying POA directly to complex multi-stage IRES planning problems still requires solving key issues such as maintaining population diversity, multi-objective non-dominated sorting and archive maintenance, and adaptive search at different stages.

Furthermore, most existing studies have placed energy system planning within static or short-term analysis frameworks, failing to explicitly model the dynamic evolution of energy demand preferences and investment capabilities of rural economies across multiple development stages, such as poverty alleviation, basic electrification, and industrial upgrading. This results in planning schemes being difficult to adapt to different strategic goals at different stages (Chen *et al.* 2023). Although heuristic algorithms have been widely applied in IRES planning, their search strategies are typically fixed or only adjusted simply based on the number of iterations. This limits their ability to perceive and respond to the dynamic changes in target weights and constraint boundaries across different economic development stages. Moreover, existing approaches lack mechanisms that embed macro-stage information into the adaptive process of the optimization algorithm (Nassar *et al.* 2025). Existing studies mostly use scenario analysis to depict short-term uncertainties, but lack systematic handling of the uncertainty of target priorities and constraint conditions at each stage over a 10-20 year planning period, and fail to provide a planning framework that can be rolled out for adjustment and adaptive correction (Zhang *et al.* 2025).

To realize low-carbon, economical, and efficient collaborative planning of IRES in the context of dynamic economic development, this study constructs an IRES multi-objective dynamic planning model integrating Economic Development Stage Division (EDSD). It uses Multiple Objective Improved POA (MOIPOA) to solve. The innovation of this research lies in: (1) By embedding the classification of macroeconomic development stages as a priori knowledge into the adaptive factors of the optimization algorithm, the search step size can be dynamically adjusted according to the evolution of the stage. This is different from the parameter adaptive mechanisms in all previous POA improvements that only rely on the number of iterations or random perturbations. Instead, the "dynamic nature of the planning problem" is transformed from a posteriori analysis to priori guidance. (2) The population initialization is carried out using the Sobol sequence combined with weak Gaussian perturbation. Compared with the chaotic mapping or good point set strategies used in existing studies, this method achieves a more uniform initial coverage in the low-dimensional decision space, which has a decisive impact on the quality of the Pareto front distribution in multi-objective optimization. (3) The integration of external archives, non-dominated sorting, and stage-adaptive position update into a unified solution framework is specifically designed for the dynamic optimization problems in IRES planning that last for 10 to 20 years and involve changes in multi-stage objective weights and constraint boundaries. Existing energy research based on POA has not addressed such long-term and phased evolution issues.

2. Related Work

2.1 Improvement and application of POA

As an emerging metaheuristic algorithm, POA has received widespread attention in complex engineering optimization problems in recent years due to its advantages of simple structure, few parameters, and easy implementation. Especially when dealing with optimization problems with multi-peak, nonlinear, and highly constrained characteristics such as energy systems, researchers have made multi-directional improvements to the basic POA. In terms of algorithm improvement strategies, recent research mainly focuses on enhancing population diversity, balancing exploration and development capabilities, and jumping out of local optimality. For example, Y. Xu *et al.* artificially improved the accuracy of photovoltaic parameter identification and used a combination of cubic chaotic mapping and refraction reverse learning strategies to initialize the population. This study introduced a catchy mutation strategy and a lens imaging reverse learning mechanism, which effectively enhanced the algorithm's global search capabilities and its ability to get rid of local extreme values (Xu *et al.*2025). Chen *et al.* (2025) proposed a multi-strategy POA to solve the NP problem of agricultural Internet of Things coverage optimization, integrating good point set strategies to expand the search range. It used the 3D spiral Lévy flight strategy to improve the convergence speed and accuracy, and enhanced the robustness to different scenarios through adaptive t-distribution variation. In the optimization of controller parameters to improve the stability of wind-solar hybrid power systems, P. Liu *et al.* improved the position update process of POA by introducing the Lévy flight strategy and overcame its local convergence problem (Liu *et al.* 2025). At the level of multi-objective expansion and engineering application, L. Yi *et al.* clearly proposed MOIPOA for the first time and used it for the dynamic reconstruction of rural rooftop photovoltaic arrays. It improved the output power while optimizing the switch life, demonstrating its potential in dealing with multi-objective trade-off problems (Yi *et al.* 2024). In system-level control and optimization, Mary *et al.* (2025) combined POA with an adaptive neuro-fuzzy inference system to optimize the power flow of hybrid power generation systems, achieving rapid stability and high energy efficiency. These studies showed that the targeted improved POA and its multi-objective variants were superior to traditional algorithms in solution accuracy, convergence speed, and robustness. This provided a strong algorithm basis for applying it to more complex multi-objective planning of IRES systems (Mary *et al.* 2025).

2.2. Research status of IES planning modeling methods

The core of IES planning is to build an optimization model that can accurately reflect the physical characteristics, economic laws and external environmental impacts of the system, and to use effective methods to solve it. In terms of modeling that considers resource characteristics and multi-factor synergy, scholars are committed to more accurately portraying the volatility and correlation of renewable energy (Yi *et al.*2024). Zhang *et al.* (2024) used the Frank-Copula function to describe the complex correlation between wind power and photovoltaic output and used two-stage robust optimization combined with K-means clustering for planning, making the planning results more consistent with local reality. What is more distinctive is the deep coupling with agricultural production. Fu *et al.* (2024) pioneered the establishment of an agricultural load model based on the physiological ecology of crop growth. They analyzed the carbon cycle within the agriculture-energy system and proposed a rural distributed energy planning model for agriculture-energy-environment synergy, achieving the unification of economic benefits and environmental benefits.

At the policy impact level, Wang *et al.* (2026) based on provincial panel data of China, using the difference-in-differences model, analyzed the impact of the new urbanization pilot policy on rural energy consumption carbon emissions. They found that this policy actually led to an average annual increase of 1.278 tons of carbon emissions per capita in rural areas, and there was a significant spillover effect. This conclusion revealed that the urbanization process may indirectly increase carbon emissions by changing the intensity and structure of rural energy consumption, indicating that simple policy intervention, if lacking complementary energy system optimization measures, may be difficult to achieve the expected emission reduction goals. Liu *et al.* (2025) examined the high-order moment risk spillover effect between the carbon market and the energy market, finding that climate policy uncertainty would significantly exacerbate the risk contagion between the two markets, especially in extreme risk states. This finding indicated that when rural systems participate in emission reduction through the carbon trading market, financial risks brought by external market fluctuations need to be guarded against. At the technical and economic feasibility level, Sakka (2025) verified the potential of ultra-low-cost anaerobic digesters (below 20 US dollars) based on household organic waste for biogas production in rural areas of Tunisia. Although the energy density of biogas is much lower than fossil fuels, its significant low-carbon emission characteristics and economic practicability provide a sustainable energy alternative for resource-poor communities.

To sum up, existing improvements in POA mostly focus on improving the performance of general test functions or solving specific engineering sub-problems. Its strategy lacks deep adaptation to the multi-stage, multi-objective, and high-constraint complexity unique to IRES system planning, and the adaptive mechanism of the algorithm fails to correlate with macroeconomic development dynamics. Secondly, although existing IES planning models continue to make progress in uncertainty processing and refined modeling, they generally place planning in a static or short-term analysis framework. It ignores the fundamental and systemic impact of regional economic development stages on planning target priorities, constraints, and investment capabilities, and lacks an endogenous dynamic evolution perspective. In response to the above shortcomings, this study proposes a planning framework that deeply integrates EDSD and MOIPOA. It divides rural economic development stages through quantitative indicators, and transforms stage characteristics into dynamic target weights and constraint boundaries in the planning model. On this basis, the basic POA is improved to enable dynamic responsiveness to change in planning preferences and feasible regions across different stages during the search process. This allows the algorithm to automatically generate a Pareto-optimal planning solution set. The resulting set is coordinated with the long-term development path of the region.

3. Research Methods

3.1 IRES modeling

The planning, adoption and transformation of energy systems is essentially a “socio-technical” process deeply embedded in specific socio-economic structures. If pure technical and economic optimization is separated from the consideration of rural social capital, community governance model, user behavior habits and institutional policy environment, it is often difficult to implement or fail to achieve expected benefits. In particular, there are significant differences in energy equity, social acceptance, and community participation capabilities in rural communities at different stages of economic development. For example, in the initial stage, fragile affordability and weak infrastructure may make energy system planning primarily address energy poverty, and its success is highly dependent on external financial subsidies and inclusive policy design. In the optimization and stabilization stage, planning needs to respond to residents’ higher demands for energy quality, environmental value and even energy democracy (Serat *et al.* 2023). Therefore, this study constructs a core model framework that can not only describe the physical characteristics and operational constraints of the energy system in rural areas, but also reflect its dynamic evolution with macroeconomic development.

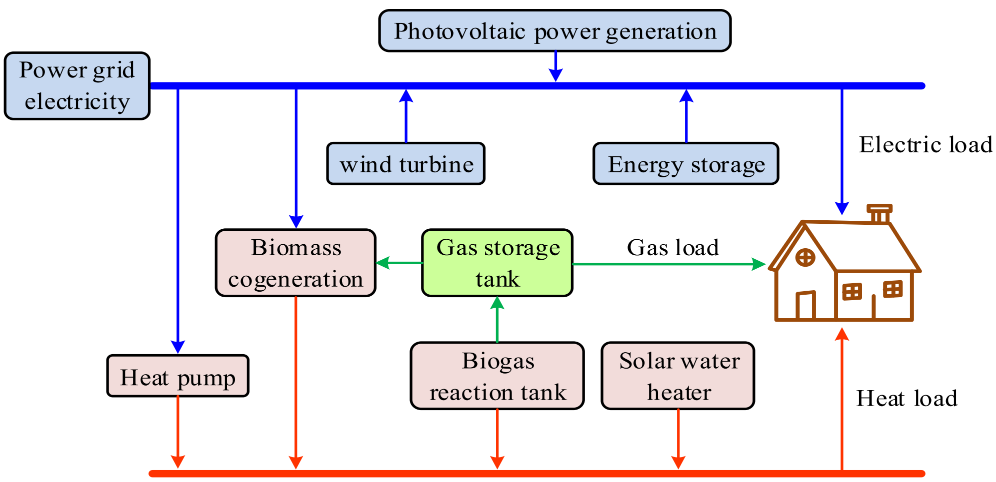

Fig. 1 IRES architecture

3.1.1 System architecture

Figure 1 is a typical IRES architecture. Its core is to realize the coordinated optimization of local renewable energy and conventional energy, energy storage devices and diversified loads. In Figure 1, the energy flow of the system mainly includes electric power flow, thermal flow and gas flow. The system converts solar and wind energy into electrical energy through photovoltaic and wind power generation. It digests agricultural waste in a biogas digester to produce biogas, which is stored in a gas storage tank and then supplied to the cooking load or biomass cogeneration unit to generate heat. Heat pumps and solar collectors convert electrical energy or solar energy into thermal energy to meet users' heating and hot water needs. Batteries are used to balance the temporal and spatial differences in power supply and demand. The system realizes two-way interaction of electric energy through the public power grid to ensure the reliability of power supply.

To achieve the quantitative division of economic development stages, this study selects three indicators: per capita regional GDP (ten thousand yuan/person), the proportion of non-agricultural industry value added in GDP (%), and the per capita electricity consumption of rural residents (kWh/person). Based on these indicators, the economic development is divided into three dynamic stages. The initial stage (where per capita GDP is less than 20,000 yuan, the proportion of non-agricultural industry in GDP is less than 60%, and per capita electricity consumption is less than 300 kWh/person) aims to address basic energy needs as the primary goal. The growth stage (where per capita GDP is between 20,000 and 50,000 yuan, the proportion of non-agricultural industry is between 60% and 80%, and per capita electricity consumption is between 300 and 800 kWh/person) sees rapid growth in demand, emphasizing reliability and economy. The optimization and stability stage (where per capita GDP is greater than 50,000 yuan, the proportion of non-agricultural industry is greater than 80%, and per capita electricity consumption is greater than 800 kWh/person) focuses on low-carbon environmental protection and overall system efficiency.

The thresholds of per capita GDP of 20,000 yuan and 50,000 yuan were based on typical divisions of the rural poverty line and the middle-income threshold in China. The proportions of non-agricultural industry of 60% and 80% correspond to the general dividing points of the early and late stages of industrialization, which are based on the basic logic of the "Charnley Industrialization Stage Model" in industrial economics. The thresholds of per capita electricity consumption of 300 kWh and 800 kWh were based on the recommended standards of the International Energy Agency for "basic electrification" and "adequate modern energy services". When a region simultaneously meets two or more threshold values of a certain stage, it is determined to enter that stage.

In the planning model, the weights and constraints of the objective function are dynamically adjusted according to the current stage to which the target area belongs. The specific adjustment method is as follows: in the initial stage, the economic goal is given the highest weight of 0.6, and the environmental protection goal has the lowest weight of 0.2. In the growth stage, the economic and reliability goals are given higher weights of 0.4 each. In the optimization and stability stage, the weights of environmental protection and efficiency goals are increased to 0.35 each. Regarding the constraints, in the initial stage, the investment upper limit is set at a relatively low value (such as 10% of the regional annual fiscal revenue) to reflect the capital constraint. In the growth stage, the investment upper limit is appropriately relaxed. In the optimization and stability stage, a lower carbon emission lower limit constraint is introduced.

3.1.2 Energy balance model

To conduct quantitative optimization analysis, it is necessary to establish accurate mathematical models for each link in the IRES system. System operation needs to meet the real-time balance constraints of electricity, heat, and gas. The electric power balance equation is shown in Equation (1).

$$\begin{aligned} &P_{grid}^{buy}(t)+P_{pv}(t)+P_{wt}(t)+P_{bchp}^{elec}(t)+P_{ees}^{dis}(t) \\ &=P_{load}^{elec}(t)+P_{hp}(t)+P_{ees}^{ch}(t)+P_{grid}^{sell}(t)++P_{loss}^{elec}(t) \end{aligned} \quad (1)$$

In Equation (1), $P_{grid}^{buy}(t)$ and $P_{grid}^{sell}(t)$ are the power (kW) purchased from the grid and sold to the grid during period t. $P_{pv}(t)$ and $P_{wt}(t)$ are the actual output (kW) of photovoltaic and wind turbines. $P_{bchp}^{elec}(t)$ is the power generation of the combined heat and power unit (kW). $P_{ees}^{dis}(t)$ and $P_{ees}^{ch}(t)$ are the discharge and charging power of the battery (kW). $P_{load}^{elec}(t)$ is the electrical load demand (kW). $P_{hp}(t)$ is the heat pump power consumption (kW). $P_{loss}^{elec}(t)$ is the system network loss (kW). The thermal power balance equation is shown in Equation (2).

$$H_{bchp}^{heat}(t)+H_{hp}(t)+H_{swh}(t)\geq H_{load}^{heat}(t)+H_{ad}(t)+H_{loss}^{heat}(t) \quad (2)$$

In Equation (2), $H_{bchp}^{heat}(t)$, $H_{hp}(t)$, and $H_{swh}(t)$ are the heat supply (kW) of the cogeneration unit, heat pump and solar collector. $H_{load}^{heat}(t)$ is the heat load demand (kW). $H_{ad}(t)$ is the heat energy (kW) required to maintain the fermentation temperature of the biogas digester. $H_{loss}^{heat}(t)$ is the heat network loss (kW). The biogas mass balance equation is shown in Equation (3).

$$G_{ad}(t)+G_{bes}^{dis}(t)=G_{load}^{gas}(t)+G_{bchp}(t)+G_{bes}^{ch}(t) \quad (3)$$

In Equation (3), $G_{ad}(t)$ is the gas production rate of the biogas pool (m^3/h). $G_{bes}^{dis}(t)$ and $G_{bes}^{ch}(t)$ are the deflation and charging rates of the gas tank (m3/h). $G_{load}^{gas}(t)$ is the cooking gas load (m^3/h). $G_{bchp}(t)$ is the gas consumption rate of the cogeneration unit (m^3/h).

3.1.3 Key equipment operation model

Photovoltaic output mainly depends on light radiation intensity and ambient temperature. The photovoltaic power generation model is shown in Equation (4).

$$\begin{cases} P_{pv}(t)=N_{pv}\cdot A_{pv}\cdot G(t)\cdot \eta_{pv}(t) \\ \eta_{pv}(t)=\eta_{pv}^{stc}\cdot[1-\alpha\cdot(T_{cell}(t)-T_{stc})] \end{cases} \quad (4)$$

In Equation (4), N_{pv} is the number of photovoltaic panels. A_{pv} is the area of the single board (m^2). $G(t)$ is the total radiation intensity of the slope (kW/m^2). $\eta_{pv}(t)$ is the actual conversion efficiency. η_{pv}^{stc} is the efficiency under standard test conditions. α is the power temperature coefficient (%/℃). $T_{cell}(t)$ is the operating temperature of the battery panel (℃). T_{stc} is the standard test temperature (℃). There is a nonlinear relationship between biogas production and the temperature in the pond, so the empirical formula can be used for fitting, as shown in Equation (5).

$$G_{ad}(t)=f(T_{ad}(t))\cdot V_{substrate} \quad (5)$$

In Equation (5), $f(T_{ad}(t))$ is the temperature-gas production rate function ($m^3/(m^3 \cdot h)$). $V_{substrate}$ is the volume of fermentation raw materials (m^3). Pool temperature dynamics are determined by the thermal power balance equation, involving ambient heat dissipation and external heating (Yu *et al.* 2025). The energy storage equipment model takes the battery as an example, and the energy storage state update equation is shown in Equation (6).

$$SOC(t) = SOC(t-1) \cdot (1-\varphi) + \left(\eta_{ch} \cdot P_{ch}(t) - \frac{P_{dis}(t)}{\eta_{dis}}\right) \cdot \frac{\Delta t}{E_{rated}} \tag{6}$$

In Equation (6), $SOC(t)$ is the state of charge at the end of period t. φ is the self-discharge rate. η_{ch}/η_{dis} and $P_{ch}(t)$ /$P_{dis}(t)$ are charging and discharging efficiency and power (kW). E_{rated} is the rated capacity (kWh). Δt is the time interval. The above energy balance equations (1) to (3) and the key equipment operation models (4) to (6) are all standard mathematical descriptions widely used in the field of comprehensive energy system planning. They mainly refer to the classic modeling framework in this field and have been improved accordingly.

3.2 IRES operation optimization based on MOIPOA

POA is a metaheuristic algorithm that simulates the hunting behavior of pelican groups. It has the advantages of simple structure, few parameters, and easy implementation. However, standard POA is a single-objective optimization design and is directly applied to complex multi-objective optimization problems such as IRES systems. It has limitations such as volatile population diversity, insufficient Pareto front convergence and distribution, and difficulty in balancing multi-stage searches (Song *et al.* 2025). To this end, this study proposes a MOIPOA.

3.2.1 Population initialization strategy based on Sobol sequence

Standard POA uses a pseudo-random number generator to randomly initialize the population in the search space, which may lead to uneven distribution of initial individuals, affecting the global search efficiency of the algorithm and the diversity of the final solution set (He *et al.* 2025; Mohan *et al.* 2025). To improve the uniformity and ergodicity of the initial population in the decision space, this study uses Sobol quasi-random sequence instead of the pseudo-random number generator for initialization, and introduces weak Gaussian perturbation to maintain the necessary randomness.

The Sobol sequence is a low-difference sequence, and the value $x_n^{(j)}$ of the nth point in the jth dimension is generated by the direction number $v_i^{(j)}$, as shown in Equation (7).

$$x_n^{(j)} = n_1 v_1^{(j)} \oplus n_2 v_2^{(j)} \oplus \ldots \oplus n_i v_i^{(j)} \tag{7}$$

In Equation (7), $\oplus$ is a bitwise XOR operation, and n_i is the ith bit of the binary representation of n. To enhance the robustness, Gaussian noise with a mean of 0 and a standard deviation of σ is added to the generated Sobol sequence points, as shown in Equation (8).

$$P_{init}(i,j) = x_i^{(j)} \cdot (up_j - low_j) + low_j + \mathrm{N}\ (0, \sigma^2) \tag{8}$$

In Equation (8), $P_{init}(i,j)$ is the initial value of the ith individual on the jth dimension decision variable. $[low_j, up_j]$ is the search boundary. Figure 2 shows the comparison of the effects of population initialization strategies.

In Figure 2, compared with random initialization, Sobol sequence initialization can make the population more evenly distributed in the search space and provide a more comprehensive starting point for subsequent searches. The standard POA initializes the population using a pseudo-random number generator, and the expected distribution difference of the population in the decision space is $E[D_{\text{rand}}] = O(1/\sqrt{N})$, where N is the population size. The Sobol sequence is used as a low-difference sequence, with a difference $D_{\text{Sobol}} = O((log\,N)^d/N)$, and d is the dimension of the decision variables. When d is small (in this study, $d \leq 10$), the theoretical difference of the Sobol sequence is significantly lower than that of the pseudo-random initialization. This means that the initial population can more evenly cover the feasible region, thereby reducing the probability of the algorithm getting stuck in local optimum and providing more abundant initial Pareto candidate solutions for the subsequent non-dominated sorting.

3.2.2 External archives and non-dominated sorting mechanism for multi-objective optimization

To extend single-objective POA to multi-objective fields and effectively manage and maintain Pareto optimal solution sets, MOIPOA introduces external files and a fast non-dominated sorting mechanism. The external archive is an

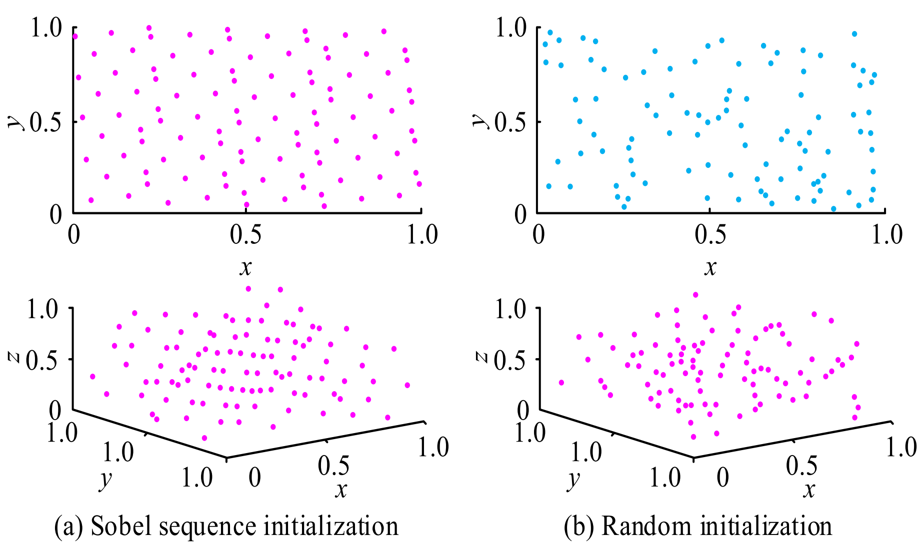

Fig 2 Population distribution under the two initialization methods

independent repository used to save and update the non-dominated solutions discovered so far during the iterative process (Ma *et al.* 2025). The file capacity N_A is fixed. After each population update, the newly generated non-dominated solutions are merged with the historical solutions in the archive. When the number of combined non-dominated solutions exceeds N_A, pruning is required. First, fast non-dominated sorting is used to divide the solution set into multiple frontier levels (Frontier Rank, R1, R2,…). Among them, R_1 is the Pareto front with the highest non-dominated level. Then, the crowding distance cd_i of each solution i within the same frontier level is calculated to measure the distribution density of the solution on its frontier, as shown in Equation (9).

$$cd_i = \sum_{m=1}^{M} \frac{|f_m(i+1) - f_m(i-1)|}{f_m^{max} - f_m^{min}} \tag{9}$$

In Equation (9), M is the number of objective functions. $f_m(i)$ is the value of solution i on the m −th target, and the solutions need to be sorted according to this target value. The larger the crowding distance, the smaller the density around the solution and the better the diversity. The file maintenance strategy is to give priority to retaining solutions in the high-ranking front R_1. If the number of solutions in R_1 exceeds the file capacity, the solutions with larger crowding distance will be retained.

3.2.3 Integration stage information and ADF position updates

In the position update formula of the standard POA "moving toward prey" (exploration phase), parameter λ is usually randomly set to 1 or 2. This fixed or random strategy may not be able to adaptively balance global exploration and local development when dealing with complex multi-stage, multi-modal optimization problems. To this end, this study introduces an Adaptive Dynamic Factor (ADF) μ associated with the iterative process and economic development stage in POA to replace the original λ. First, the basic adaptive factor is defined as $\mu_{base}(t)$, which adaptively decreases as the number of iterations t increases, as shown in Equation (10).

$$\mu_{base}(t) = \mu_{max} - (\mu_{max} - \mu_{min}) \times \left(\frac{t}{T_{max}}\right)^{\gamma} \tag{10}$$

In Equation (10), μ_{max} and μ_{min} are the upper and lower limits of the factor, T_{max} is the maximum number of iterations, and γ is the parameter that adjusts the shape of the curve. This ensures that the algorithm tends to global exploration (larger μ) in the early stage and local development (smaller μ) in the later stage.

More importantly, to enable the algorithm to perceive and adapt to the staged characteristics of rural energy system planning, this study incorporates the stage impact factor $\phi(s)$ into it. Different search biases are given according to the economic development stage s to which the current plan

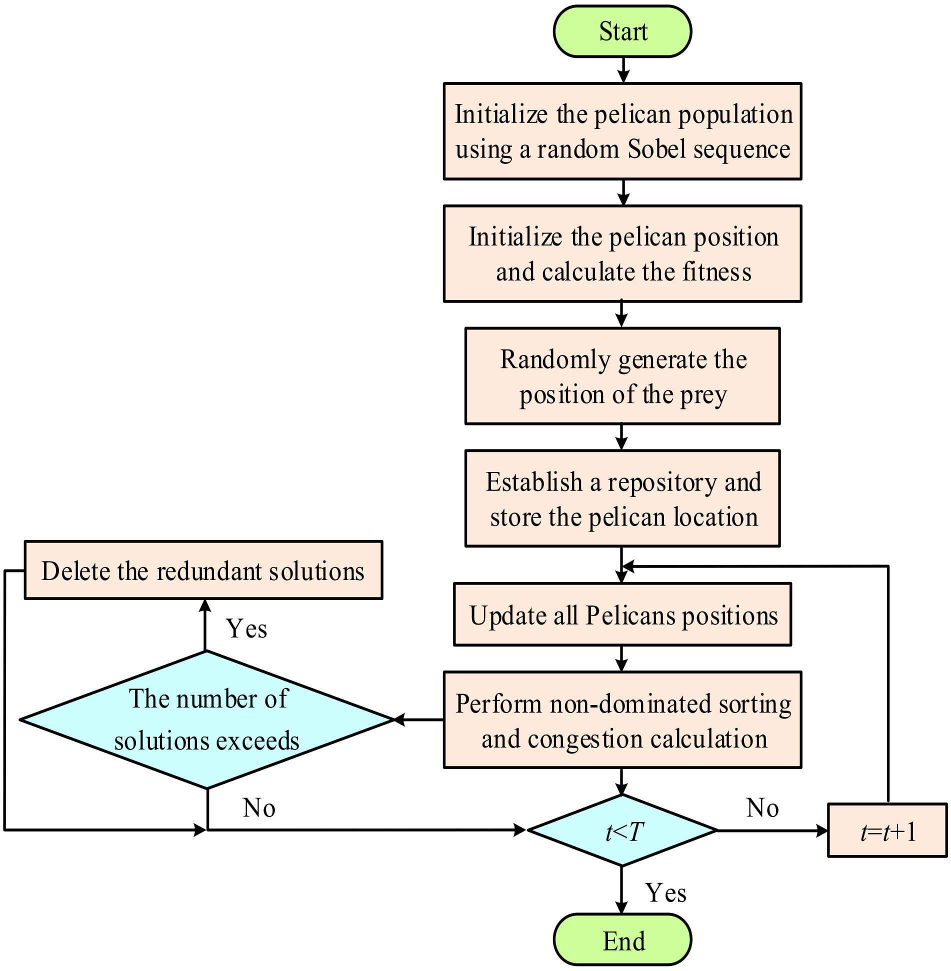

Fig 3 MOIPOA process

belongs. For example, in the early stages of economic development, it is necessary to emphasize quickly finding feasible solutions, and $\phi(s)$ can be set to make the search more exploratory. In the later stage of economic development, the emphasis is on fine search, and $\phi(s)$ can be set to enhance development capabilities. The final ADF $\mu(t,s)$ is shown in Equation (11).

$$\mu(t,s) = \phi(s) \cdot \mu_{base}(t) \tag{11}$$

The step size factor of the standard POA during the exploration stage is randomly set as $I \in \{1,2\}$, lacking adaptive adjustment of the search process. The ADF $\mu(t,s)$ proposed in this study is defined as $\mu_0(t) \cdot \gamma(s)$, where $\beta_0(t)=\beta_{max}-(\mu_{max}-\mu_{min})\cdot(t/T_{max})^k$ decreases monotonically and $\gamma(s)$ is adjusted according to the economic development stage. According to the random approximation theory, when the step size factor satisfies $\sum_{t=1}^{\infty} \mu(t) = \infty$ and $\sum_{t=1}^{\infty} \mu^2(t) < \infty$, the random search algorithm converges to the global optimal neighborhood with probability 1. In this design, $\mu(t)$ decays with the increase of the number of iterations (due to $\mu_0(t)$ decreasing and $\gamma(s)$ being a normal number), meeting the above convergence conditions. Meanwhile, the stage factor $\gamma(s)$ enables the algorithm to maintain an appropriate step size scale in different optimization stages, avoiding premature convergence to local optima or oscillation in the later stage. The improved pelican position update formula (exploration phase) is shown in Equation (12).

$$P_{i,j}^{t+1} = \begin{cases} P_{i,j}^t + rand \cdot (S_j^t - \mu(t,s) \cdot P_{i,j}^t), & \text{if } \mathbf{F}(\mathbf{S}^t) \prec \boldsymbol{F}(\boldsymbol{P}_i^t) \\ P_{i,j}^t + rand \cdot (P_{i,j}^t - S_j^t), & \text{otherwise} \end{cases} \tag{12}$$

In Equation (12), $\prec$ is the position of the i −th pelican (individual) of the tth generation in the jth dimension. S_j^t is the position in the j th dimension of the "leading prey" (one of the global optimal solutions) selected from the current external file based on crowding or roulette strategy. $\boldsymbol{F}$ is the objective function vector. $\prec$ is a Pareto dominance relationship. The adaptive factor $\mu(t,s)$ dynamically adjusts the step length for individuals to learn from the leader, achieving collaborative adaptation of the search strategy and problem stage characteristics. Based on the above improvements, the main process of MOIPOA applied to IRES multi-stage planning is shown in Figure 3.

In Figure 3, MOIPOA first uses Sobol sequence combined with Gaussian perturbation to initialize the population to improve the uniformity and diversity of the initial solution in the decision space. The next step is to enter the main loop, and in each generation, the algorithm updates the individual position through the ADF incorporating stage information, dynamically balancing global exploration and local development. After each round of iteration, the newly generated non-dominated solutions are merged with the archive historical solutions, and the fast non-dominated sorting and crowding distance mechanisms are used to maintain and update the archives, retaining solutions with high frontier levels and good distribution. Finally, after reaching the maximum number of iterations, the Pareto optimal solution set in the external file is output.

The main computational costs of MOIPOA include population initialization, position update, non-dominated sorting, and external archive maintenance. Let the population size be N, the maximum number of iterations be T, the number of objective functions be M, and the size of the archive be A. The complexity of Sobol sequence initialization is $O(Nd)$, which is of the same order as random initialization. The complexity of position update in each generation is $O(Nd)$. The non-dominated sorting uses fast non-dominated sorting, with the worst complexity of $O(MN^2)$, but in actual operation, due to the adoption of elite retention and archive pruning, the average complexity is approximately $O(MN\,log\,N)$. The complexity of calculating the crowding distance in archive maintenance is $O(MA\,log\,A)$. Therefore, the total time complexity of MOIPOA is $O(T(MN^2 + MA\,log\,A + Nd))$. Compared with the standard POA (single objective, complexity $O(TNd)$), MOIPOA increases the cost of non-dominated sorting due to handling multiple objectives, but it is at the same level as similar multi-objective algorithms (such as NSGA-II, complexity $O(TMN^2)$).

3.3 Multi-objective dynamic programming of integrated stage division

IRES planning is not a static problem, and its optimal configuration and operation strategy are deeply dependent on the macroeconomic development process of the region (Dong *et al.* 2023; Mu *et al.* 2024). To achieve the collaborative optimization of IRES in each economic development stage, this study constructed a multi-objective dynamic programming model integrating stage division. The model adopts a two-stage stochastic planning framework to explicitly depict the coupling relationship between planning decisions and operation scheduling, and to systematically handle the uncertainty of comprehensive energy output and load demand. The overall framework of the model is shown in Figure 4.

In Figure 4, the first stage (planning stage) determines the long-term configuration capacity of various types of energy equipment. The second stage (operation stage) optimizes the equipment output, energy storage status and real-time electricity price strategy in typical days under a given capacity to minimize operating costs. The two stages are related to each other through capacity variables and operation cost functions, and jointly pursue the dual goals of minimizing the economic cost of the entire life cycle of the system and maximizing CER benefits (Wang *et al.* 2025).

3.3.1 Objective function

IRES is not a static issue. Its optimal configuration and operation strategy are highly dependent on the regional macroeconomic development process, and are also affected by multiple uncertain factors such as renewable energy output, electricity market prices, and long-term economic growth. To achieve the coordinated optimization of IRES under different economic development stages, this study adopts a two-stage stochastic programming framework for unified treatment. The two stages are interconnected through capacity variables and operation cost functions, jointly pursuing the dual goals of minimizing the equivalent annualized total cost of the system over its entire life cycle and maximizing the annual net carbon emission reduction (CER). The modified expected form objective function is shown in Equation (13).

$$\begin{cases} min\,E\,[C_{\text{total}}] = \sum_{s=1}^{S} \pi_s \cdot C_{\text{total},s} \\ max\,E\,[E_{\text{reduce}}] = \sum_{s=1}^{S} \pi_s \cdot E_{\text{reduce},s} \end{cases} \tag{13}$$

In Equation (13), S represents the total number of scenarios, π_s represents the occurrence probability of scenario s, and $C_{\text{total},s}$ and $E_{\text{reduce},s}$ respectively represent the system's equivalent annualized total cost and annual net CER under scenario s.

For renewable energy output uncertainty, the Frank-Copula function is used to capture the nonlinear spatiotemporal correlation of photovoltaic and wind power output, generating hourly wind and solar power sequences covering 8,760 hours annually. This addresses the limitation of traditional

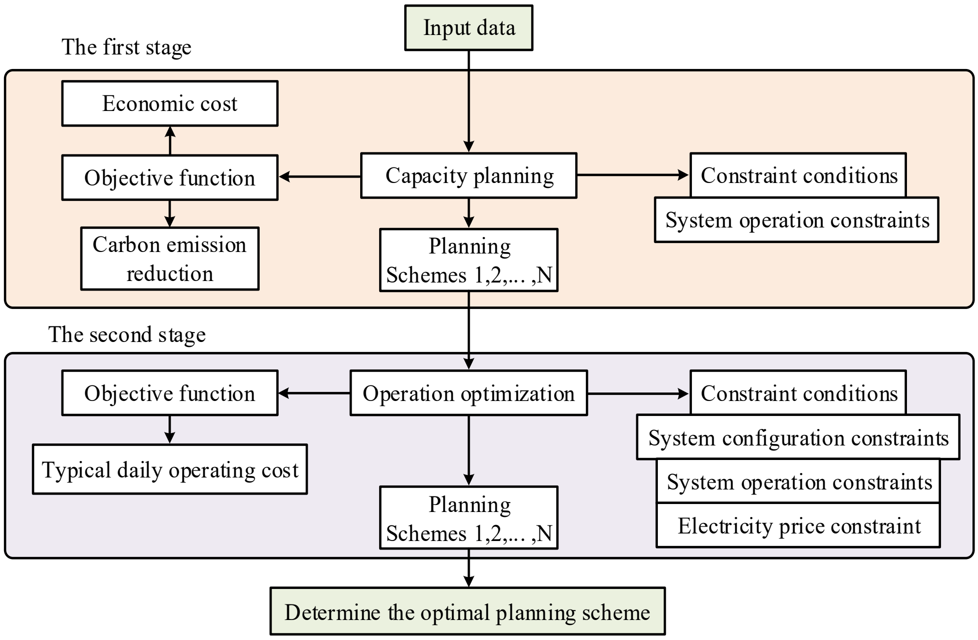

Fig 4 Basic framework of multi-objective two-stage stochastic programming

independent random generation methods in capturing wind-solar complementarity. For power market uncertainty, the geometric Brownian motion model simulates random fluctuations of time-of-use electricity prices, calibrated against historical local market data from 2020 to 2024. Peak, flat, and off-peak price volatilities are set at 15%, 10%, and 8%, respectively, to generate typical operation scenarios under different price levels. Long-term economic fluctuations are captured through the proposed multi-stage economic development classification mechanism, defining three scenarios: low growth (3% average annual GDP growth), benchmark growth (5%), and high growth (7%). Each scenario corresponds to distinct energy demand growth rates, investment budget caps, and target weight coefficients, enabling dynamic adaptation of the planning scheme to the long-term economic development path.

3.3.2 Constraints

To ensure the feasibility, safety and economy of the proposed planning scheme, the IRES multi-objective two-stage stochastic programming model is constructed. Its constraints mainly cover system equipment configuration capacity constraints, system operation constraints and electricity price constraints. Among them, system operation constraints are used to ensure the real-time safe and stable operation of the system in any typical scenario and scheduling period, and mainly include energy balance models and key equipment operation models. System equipment configuration capacity constraints stipulate the upper and lower limits of the installation capacity of various types of energy equipment in the planning stage to ensure that investment is within the scope of technical feasibility and budget permission. The planned capacity of all equipment must satisfy Equation (15).

$$M_i^{\min} \le M_i \le M_i^{\max}, \quad \forall i \in \Omega_I \tag{15}$$

In Equation (15), Ω_I is a collection of equipment, including wind turbines, photovoltaic units, biogas digesters, cogeneration units, electric boilers, batteries, thermal storage tanks and gas storage tanks. M_i is the planned capacity of equipment i. M_i^{min} and M_i^{max} are the technical lower and upper limits of its capacity. In addition, the total investment needs to satisfy the budget constraint shown in Equation (16).

$$\sum_{i\in\Omega_I} M_i \cdot c_i^{\text{inv}} \le B^{\max} \tag{16}$$

In Equation (16), c_i^{inv} is the unit capacity investment cost of equipment i. $B^{\max}$ is the maximum allowable total investment. To guide user-side demand response, optimize system operation, and protect user interests at the same time, the internal real-time electricity price is constrained in the model, as shown in Equation (17).

$$\rho^{e,\min} \le \rho_t^e \le \rho^{e,\max}, \quad \forall t \tag{17}$$

In Equation (17), ρ_t^e is the electricity sales price to the user side during period t. $\rho^{e,min}$ and $\rho^{e,max}$ are the lower and upper limits of electricity prices allowed by policy or market. This constraint ensures that the price mechanism functions within a reasonable range and avoids extreme electricity prices.

3.3.3 Model solving and decision-making process

For this multi-objective, nonlinear, and uncertain two-stage planning model, this study uses MOIPOA for solution and decision-making. The process is shown in Figure 5. The process consists of three core steps. First, a probabilistic model based on scenery resources generates a large number of initial scenes, and uses the synchronous back-substitution method to reduce them to a representative set of typical scenes to characterize uncertainty. Then, MOIPOA jointly encodes planning variables and key operational variables, and continuously updates the population by simulating the flight and siege behaviors of pelicans in iterations. In each generation, the operational optimization sub-problems in all typical scenarios are solved for each individual, its economic cost and CER amount are calculated, and the Pareto optimal solution set is maintained through non-dominated sorting. After obtaining the Pareto

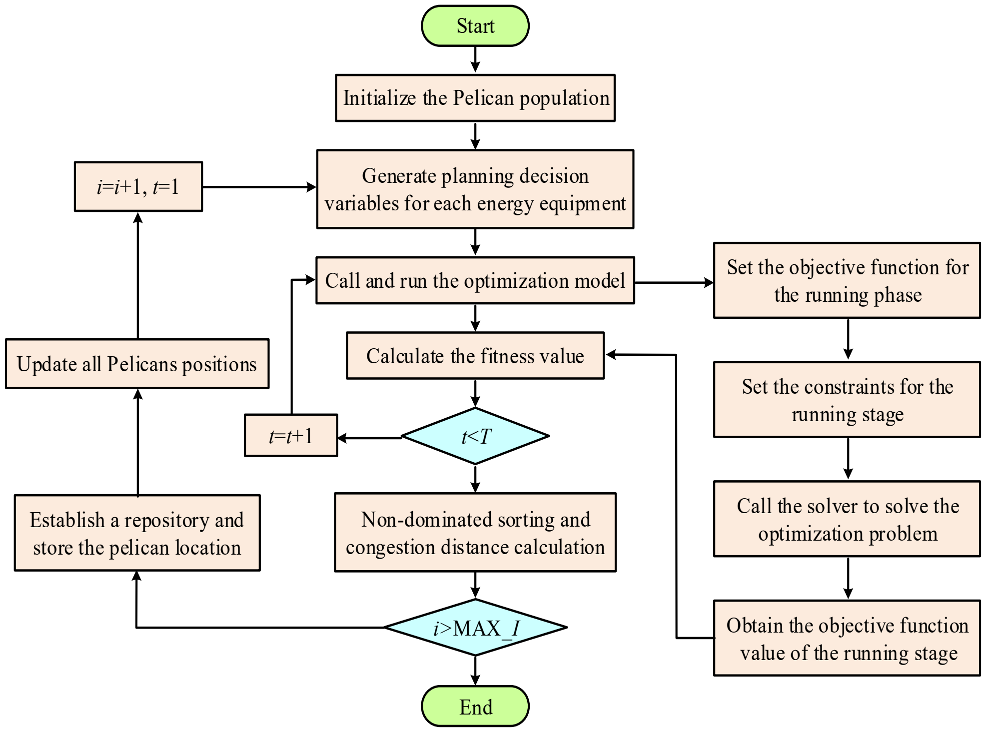

Fig 5 IRES planning and operation of the two-layer optimization model solution process

front, the distance method of superior and inferior solutions was used to make the final decision. Decision makers can set target weights based on local development priorities and automatically select planning solutions that best meet needs from the Pareto solution set.

4. Experimental Results

4.1 Experimental setup

This study took a typical rural area in northern China as the planning object. The area is rich in solar energy resources, with an average annual sunshine hour of 2,542 h and an average annual wind speed of 7.62 m/s. It has stable agricultural waste (such as straw, livestock and poultry manure) resources and a total usable biomass of about 5,000 tons per year. It has good conditions for the development of distributed clean energy. The existing power grid structure in rural areas is relatively weak, and there is a large thermal and electricity load gap during the heating season. There is an urgent need to optimize the energy structure and improve energy supply reliability and economy. The comprehensive settings of key basic parameters, economic parameters and optimization algorithm parameters involved in the planning model are shown in Table 1.

This study used MOIPOA to solve the established planning model. The parameters were set as follows: population size 150, maximum number of iterations 200, proportion of elite individuals 0.2, external file size 100, used to store non-dominated solutions generated during the iteration process. The simulation experiment was completed on a computer equipped with an Intel Core i7-12700H processor and 32GB of memory. All modeling and algorithm programs were developed and run on the MATLAB R2021a platform, and its optimization toolbox was called for auxiliary calculations. The annual hourly solar radiation, electrical load, and heat load data based on the simulation were all derived from actual observations and

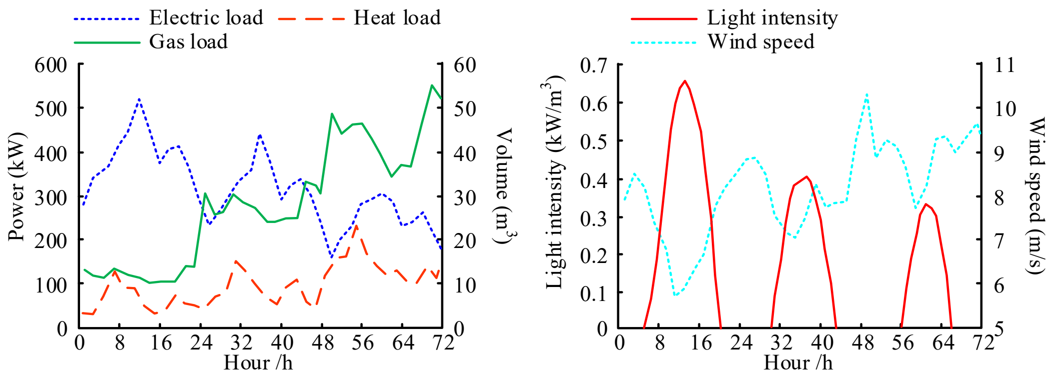

(a) Electricity, heat and gas load data

(b) Typical daily wind speed and light intensity data

Fig 6 Typical daily profiles of loads and renewable resources in the studied rural area

Table 1
Economic and technical parameters of IRES equipment

Parameter		Value	Parameter		Value
Planning the life cycle		20 years	Biomass biogas	Unit investment cost	17500 yuan/kW
Discount rate		0.08		Operation and maintenance costs	0.88 yuan/kW
Inflation rate		0.04		Power generation efficiency	50%
Grid power purchase - Off-peak price (Period: 23:00- 7:00 the next day)		0.35 yuan/kWh		Waste heat utilization efficiency	40%
Grid power Purchase - Parity (Time period: 11:00-19:00)		0.52 yuan/kWh	Ground source heat pump	Unit investment cost	17000 yuan/kW
Grid power purchase - Peak price (Time periods: 7:00-11:00, 19:00-23:00)		0.56 yuan/kWh		Operation and maintenance costs	0.80 yuan/kWh
Photovoltaic	Unit investment cost	4500 yuan/kW		Coefficient of heating performance	5.8
	Operation and maintenance costs	0.32 yuan/kWh	Electric boiler	Unit investment cost	1700 yuan/kW
	Photoelectric conversion efficiency	18.50%		Operation and maintenance costs	0.82 yuan/kWh
Solar thermal power generation	Unit investment cost	24000 yuan/kW		Electric-thermal conversion efficiency	95%
	Operation and maintenance costs	0.85 yuan/kWh	Lithium battery energy storage	Unit investment cost	1600 yuan/kWh
	Light-thermal conversion efficiency	40%		Operation and maintenance costs	0.30 yuan/kWh
Solar thermal storage system	Unit investment cost	4800 yuan/kWh		Charging/discharging efficiency	95%/95%
	Heat storage/release efficiency	95%/95%	Biogas storage tank	Unit investment cost	1650 yuan/m3

statistical data in the village, and were divided into three typical days in summer (0-23h), transition season (24-47h), and winter (48-72h), as shown in Figure 6. In Figure 6(a), the power load was relatively stable, but there were obvious morning and evening peaks. The heat load showed strong seasonality, with demand in winter being much higher than in summer and transition seasons, and with significant intraday fluctuations. Biogas load was relatively stable. In Figure 6(b), wind and solar resources showed significant complementary characteristics in both seasons and days. Summer had abundant light and low wind speed, while winter had strong wind and insufficient light. The two were relatively balanced in the transition season.

4.2 Performance analysis of MOIPOA

To verify the performance of MOIPOA, this study also uses Non-dominated Sorting Genetic Algorithm II (NSGA-II) (Kocaturk *et al.* 2025) and Multi-objective Particle Swarm Optimization (MOPSO) (Liu *et al.* 2025) for comparative analysis to ensure the effectiveness and robustness of the planning results. To ensure the fairness of the algorithm comparisons, the three algorithms adopted the same population size (150), maximum number of iterations (200), and external archive capacity (100). For the parameters specific to each algorithm, they were independently tuned through grid search. In NSGA-II, the crossover probability was set to 0.9 and the mutation probability was set to 1/decision variable dimension. In MOPSO, the inertia weight decreased linearly from 0.9 to 0.4, and the learning factors c_1 and c_2 were both set to 1.5. In MOIPOA, the upper and lower limits of the adaptive factor were 0.9 and 0.2 respectively, and the shape parameter k was set to 2. All algorithms were run on the same hardware environment and the MATLAB R2021a platform.

Table 2 summarizes the average values (Mean) and standard deviations (Std) of the inverse generational distance (IGD) and spacing (SP) indicators obtained by MOIPOA, NSGA-II, and MOPSO after running 30 times on the ZDT1 to ZDT6 test functions. For the ZDT2, ZDT3, and ZDT6 functions, the mean IGD values of MOIPOA (2.70E-03, 2.92E-03, 2.20E-03) were lower than those of NSGA-II and MOPSO, indicating that the obtained solution set was closer to the true Pareto front. In the SP indicator, MOIPOA achieved the lowest mean values on all four functions. To evaluate the credibility of the results, the 95% confidence intervals of the mean values of each indicator for 30 independent runs were calculated. Taking the IGD indicator of ZDT1 as an example, the confidence interval of MOIPOA was [2.48E-03, 2.56E-03], while that of NSGA-II was [3.73E-03, 3.97E-03], with no overlap, indicating that the difference was statistically significant.

The study also used the Wilcoxon signed-rank test to conduct pairwise comparisons of the IGD and SP indicator results from 30 independent runs, with a significance level of $\alpha = 0.05$. The test results showed that the differences between MOIPOA and NSGA-II, and between MOIPOA and MOPSO, were all statistically significant (p values are all less than 0.01) on all 5 ZDT test functions. In addition, the average single-run times of the three algorithms (taking ZDT4 as an example) were calculated: MOIPOA was 28.6s, NSGA-II was 25.3s, and MOPSO was 22.1s. The running time of MOIPOA was slightly higher than the comparison algorithms, mainly due to the additional computational overhead brought by Sobol sequence initialization and ADFs, but it was still within an acceptable range.

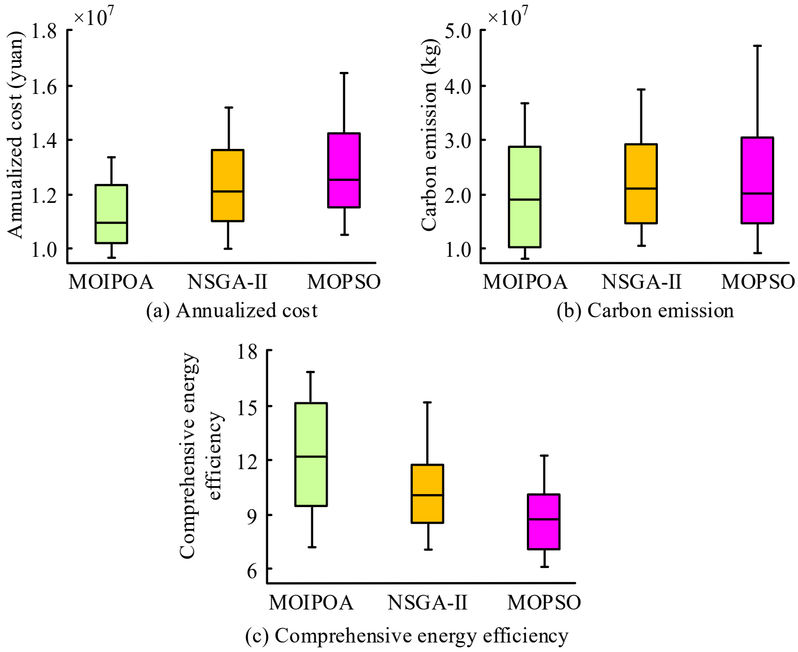

Fig 7 Performance comparison of MOIPOA, NSGA-II, and MOPSO for the IRES planning problem

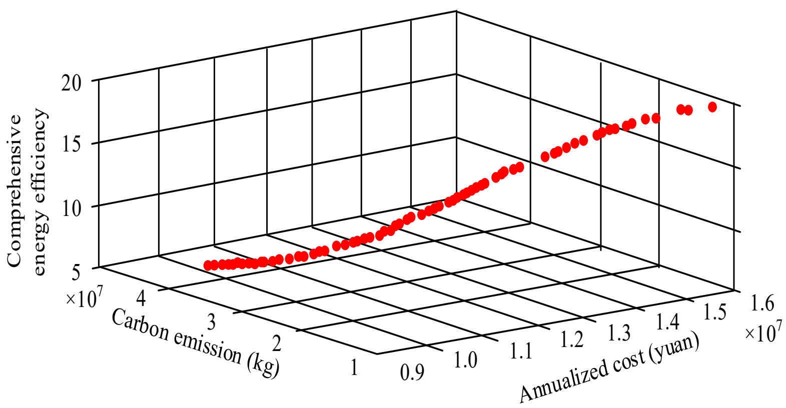

Fig 8 Three-dimensional Pareto front obtained by MOIPOA for the IRES planning problem

To evaluate the performance of different algorithms in solving the IRES multi-objective optimization problem, this study compared the solution results of MOIPOA, NSGA-II, and MOPSO. Figure 7 is a performance comparison through box plots. In Figure 7(a), in terms of economic goals, the average annualized cost of MOIPOA was 10.32 million yuan, which was better than NSGA-II's 11.23 million yuan and MOPSO's 11.56 million yuan. In Figure 7(b), the average level of CEs achieved by MOIPOA was 45,800 tons, which was significantly lower than NSGA-II's 60,150 tons and MOPSO's 65,400 tons. In terms of overall energy efficiency, MOIPOA was also ahead of NSGA-II and MOPSO. In addition, MOIPOA's solution set distribution range was wider for the two goals of CEs and comprehensive energy efficiency. MOIPOA performed better in both solution quality and solution set distribution and could better coordinate the multiple planning goals of economy, low carbon, and efficiency.

Figure 8 is the 3D Pareto front of MOIPOA. The point clouds in the figure were widely distributed along the plane composed of costs and CEs, indicating that there were a large number of transition options from high carbon and high cost to low carbon and high cost. In particular, in areas where annualized costs ranged from 12 million yuan to 15 million yuan and CEs ranged from 40,000 tons to 50,000 tons, the solution set showed significant dispersion in terms of comprehensive energy efficiency. This showed that within this cost and emission range, decision makers could still significantly improve energy efficiency by optimizing system structure and operation strategies. The few solution points located at the boundaries of the Pareto front demonstrated the potential to approach the global optimum of three objectives at the same time, providing a key extreme reference solution for multi-objective decision-making.

Table 3 shows the performance comparison of MOIPOA, NSGA-II and MOPSO in solving the IRES multi-objective programming problem. In terms of economy, the annual average total cost of the MOIPOA system was 1485.6 million yuan, which was 2.5% lower than that of NSGA-II and 4.9% lower than that of MOPSO. In terms of environmental benefits, the corresponding annual net CER of MOIPOA was 634.2 tons, which was 3.7% higher than that of NSGA-II and 7.0% higher than that of MOPSO. In terms of the comprehensive

Table 3
Performance of different optimization algorithms

Optimization algorithm	MOIPOA	NSGA-II	MOPSO
The total annual cost of the system (in ten thousand yuan	1485.6	1523.1	1558.4
Annual CEs of the system (tons)	634.2	658.7	681.5
Comprehensive energy efficiency (%)	76.8	74.1	72.5
Pareto solution set distribution (SP)	0.082	0.105	0.121
Comprehensive ranking	1	2	3

energy efficiency of the system, MOIPOA achieved 76.8%, which was 2.7% higher than that of NSGA-II and 4.3% higher than that of MOPSO. In addition, the Pareto solution set distribution index SP of MOIPOA was 0.082, which was lower than 0.105 of NSGA-II and 0.121 of MOPSO, indicating that the solution set of MOIPOA was more evenly distributed in the target space and can provide decision-makers with more balanced trade-off options. The paired t-test results showed that the above performance differences were statistically significant at the 95% confidence level ($p<0.05$), indicating that MOIPOA had statistically significant performance advantages in solving the rural comprehensive energy system planning problem of this study.

4.3 Case study

Figure 9 shows the output analysis of each equipment of the optimal compromise scheme IRES system. In Figure 9(a), photovoltaic power generation output reached its peak in summer, while wind turbine output was relatively low. In the transition season and winter, wind turbine power generation significantly exceeded that of photovoltaics. The battery maintained stable operation during most of the day and served as the base load power supply to ensure the safety of the system's energy supply. The system only purchased a small amount of electricity from the grid during a few peak hours in winter, and continued to sell electricity to the grid during daytime periods when there was sufficient sunlight or strong wind, achieving optimal energy allocation and economic benefits. Thanks to abundant and cheap local renewable energy, system-driven heat pumps consumed a large amount of electricity for heating, reflecting the cost advantages of electricity substitution. In Figure 9(b), the air source heat pump was the main heat source of the system, and its heating power accounted for the majority of the heating load, confirming its high efficiency and economy. The output of the solar collector was strictly limited by sunlight conditions, and the heat supply was limited. It mainly provided auxiliary heat energy during the noon period. The biomass cogeneration unit served as a reliable peak shaving and backup heat source, taking on the remaining heating gap when the heat pump and solar collector were insufficient. Its operation mode highlighted the role of support equipment in multi-energy complementary systems. In Figure 9(c), the gas production rate of the biogas digester showed a strong correlation with the ambient temperature. The gas production was large in summer when the temperature was higher, but the gas production decreased significantly in winter. The biogas generated was given priority to meet the cooking load of villagers, and the remaining balance was stored in gas storage tanks or used to drive cogeneration units to generate heat, realizing the cascade and recycling of biomass resources.

Figure 10 shows the operating results of the gas tank and battery. In Figure 10(a), in the spring and transition season, the gas storage tank showed frequent daily charging and deflating cycles, actively consuming the surplus biogas output during this

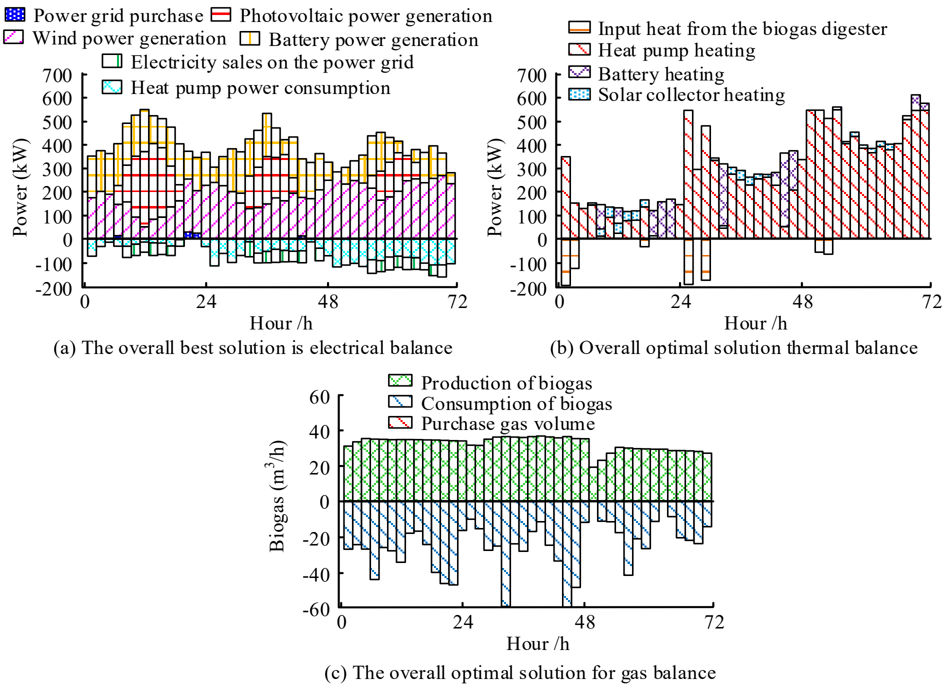

Fig. 9 Hourly output of major equipment in the optimal compromise solution over three typical days

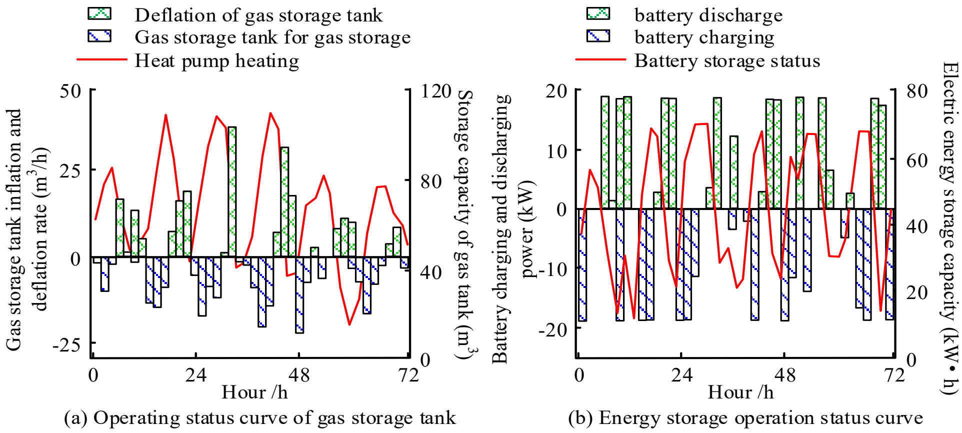

Fig 10 Operational states of the gas storage tank and battery in the optimal compromise solution

Table 4
Comparison of the optimization results of the optimal total cost, the optimal total CE, and the optimal compromise scheme

Indicator	Optimal compromise solution	Optimal total cost plan	The optimal solution for total CEs
CEs (t)	68.15	94.72	42.38
Construction cost (10,000 yuan)	95.28	82.45	118.63
Operating cost (10,000 yuan)	3.12	2.68	3.85
Total photovoltaic capacity (kW)	556.59	531.65	575.78
Total capacity of fan (kW)	450	450	450
Biomass co-generation (kW)	400	400	400
Solar collector capacity (kW)	60.5	125.3	18.75
Capacity of air source heat pump (kW)	125	125	115
Battery capacity (kWh)	112.5	187.5	37.5
Storage tank capacity (m3)	180	90	0
Capacity of biogas digester (m3)	2400	1800	3600

period. In winter, with the decline in biogas production and the increase in demand for cogeneration units, the gas storage tank switched to mainly venting, which effectively alleviated the tight gas source and ensured the continuous and stable operation of the system. In Figure 10(b), the electric energy storage equipment strictly implements the peak-valley arbitrage strategy based on time-of-use electricity prices. During a typical daily cycle, the battery completes an average of two complete charge and discharge cycles. It charges at night when electricity prices are low and when photovoltaic power is high at noon, and discharges decisively in the morning and evening when electricity prices peak. The battery's state of charge fluctuates regularly within the range of 20% to 90%. This operating mode not only smoothest the output fluctuations of renewable energy, but also significantly improves the overall economics of the system through the price difference in the power market.

The optimization results in Table 4 reveal the trade-off relationship between economic costs and CER objectives. The optimal total cost plan targets a minimum construction cost of 824,500 yuan, but its annual CEs were as high as 94.72 tons. To achieve the lowest CE of 42.38 tons, the optimal total CE plan required a construction investment of 1.1863 million yuan. The optimal compromise plan strikes a balance between the two, with a construction cost of 952,800 yuan and a CE of 68.15 tons. In terms of equipment configuration, the pursuit of low carbon requires significantly increasing the biogas digester volume to 3,600 m^3 and completely abandoning the gas storage tank. While focusing on economy, it is necessary to configure a 187.5 kW/h battery and a 125.3 kW solar collector to improve operational flexibility. The compromise plan uses a combination of 2,400 m^3 biogas digester, 180 m3 gas storage tank and 112.5 kW/h battery, which reflects the collaborative configuration strategy under multi-objective constraints.

Figure 11 shows the range of influence of the variation in the unit investment cost of the wind turbine on the three key performance indicators of the rural integrated energy system. From Figures 11(a), 11(b), and 11(c), when the cost increases positively, the annualized cost of the system rises, while carbon emissions and the overall energy efficiency of the system decrease. For example, when the investment cost of wind power decreased by 30%, the annualized total cost of the system decreased by approximately 6.2%, the annual CER decreased by approximately 5.8%, and the overall energy efficiency increased by approximately 5.1%. When the investment cost of wind power increased by 30%, the annualized total cost of the system increased by approximately 7.5%, the annual CER increased by approximately 6.3%, and the overall energy efficiency decreased by approximately 4.5%. This indicated that reducing the cost of wind power helped to improve the overall performance of this IRES.

The study further examined the influence of carbon trading prices, battery cycle life degradation coefficients, and load prediction deviations on the optimal compromise solution. Keeping all other parameters consistent with the benchmark

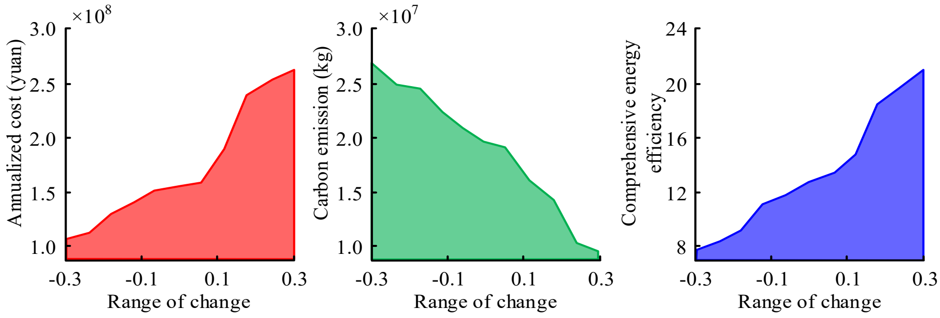

(a) Annualized cost (b) Carbon emission (c) Comprehensive energy efficiency

Fig 11 Sensitivity of system performance to wind turbine unit investment cost change

Table 5
The impact of fluctuations in different key parameters on system performance

Parameters	Scenario Setup	Annual total cost (in ten thousand yuan)	Annual carbon emission reduction (tons)
Baseline plan	-	1485.6	634.2
Carbon trading price	50% of the benchmark value	1465.3	612.5
	150% of the benchmark value	1512.8	655.8
Annual retention rate of battery capacity	95% 90%	1553.2	628.9
	Full load + 10%	1589.4	621.3
Load fluctuation	Full load - 10%	1563.8	608.4
	Scenario Setup	1433.5	657.1

scheme, carbon prices were set at 50% and 150% of the benchmark value respectively; the annual capacity retention rate of the battery was set at 95% and 90% respectively; and all loads (electricity, heat, and gas) fluctuated by 10% simultaneously. As shown in Table 5, a 50% increase in carbon trading prices led to an approximately 1.8% increase in the annualized cost, while the annual CER increased by about 3.4%. This indicated that carbon pricing had a positive incentive effect on the selection of low-carbon technologies but slightly raised the total system cost. When the annual capacity retention rate of batteries dropped to 90%, the annualized cost rose by approximately 7.0%, while the CER decreased by about 2.0%. This showed that battery degradation had a significant impact on economic performance and a relatively limited impact on environmental benefits. A 10% increase in load led to an approximately 5.3% increase in the annualized cost and a 4.1% decrease in CER. When the load decreased by 10%, the cost dropped by approximately 3.5% and the emission reduction increased by approximately 3.6%. This indicated that the system had certain robustness to load fluctuations, but both economic performance and environmental benefited deteriorate significantly in high-load scenarios. Overall, the negative impacts of battery degradation and load increase scenarios on the planning results were the most prominent. In future applications, equipment lifespan management and load prediction margins need to be considered.

5. Discussion

The MOIPOA algorithm proposed in this study demonstrated certain advantages in IRES multi-objective programming. On the ZDT test functions, the IGD mean of MOIPOA reached the lowest value of 2.20E-03, and the SP index was 4.23E-03, which were superior to the comparison algorithms. In practical cases, the annualized total cost obtained by MOIPOA was 14.856 million yuan, the annual net CER was 63.42 tons, the comprehensive energy efficiency was 76.8%, and the Pareto distribution index was only 0.082. These improvements were mainly attributed to two aspects: Firstly, the Sobol sequence initialization enabled the initial population to cover the decision space more uniformly, effectively avoiding the local optimal traps caused by random initialization. Secondly, the ADF integrated with economic development stage information enabled the algorithm to dynamically adjust the exploration and development steps according to the stage characteristics, solving the fundamental defect of traditional algorithms that the fixed search strategy cannot respond to the changes in planning preferences. In recent years, issues related to time series correlation and dynamic adaptability in the operation optimization of IES have received attention. For instance, Xu *et al.* (2026) employed a GRU-driven dynamic energy hub model to capture the nonlinear relationship between efficiency parameters and operating conditions. Different from the aforementioned data-driven approach, this paper's ADF does not rely on historical data fitting. Instead, it directly takes the evolution of the macroeconomic development stage as an external input for the algorithm parameters. The former addresses the dynamic response at the operational level, while the latter deals with the structural changes in the goals and constraints at the planning level over economic stages.

Most previous studies have placed the energy system in a static or short-term analysis framework, ignoring the structural changes in regional economies regarding energy demand preferences, investment capabilities, and carbon emission priorities during the process of poverty alleviation to industrialization upgrading. Wei *et al.* (2026) proposed an electric-hydrogen-ammonia hierarchical rolling scheduling framework, indicating that multi-level decisions across years, weeks, and days can effectively enhance the system's robustness to renewable energy fluctuations. This paper focuses on the qualitative changes in planning goals and constraints as the economic long-term development stage evolves, and divides the economy into three dynamic stages based on three indicators: per capita GDP, non-agricultural industry proportion, and per capita electricity consumption. In the initial stage, the investment upper limit is set at 10% of the regional annual fiscal revenue, and in the optimization stability stage, a stricter carbon emission lower limit is introduced. This linkage mechanism between the economic stage and planning parameters enables the optimization results to truly reflect the core contradictions of different development periods. The initial construction cost of the optimal compromise solution was 952,800 yuan, with carbon emissions of 68.15 tons. While the pure economic optimal solution reduced the cost to 824,500 yuan, the carbon emissions were as high as 947.2 tons. In the early stage of economic development, if only pursuing low costs, carbon emissions would increase significantly, while the low-carbon solution costed 1,186,300 yuan and had carbon emissions of 42.38 tons, which was difficult to bear in poverty-stricken areas.

The carbon trading price had a significant regulatory effect on the system's economy and the reduction of emissions. Zhang et al. (2026) found in the low-carbon scheduling of the integrated energy system that the stepped carbon trading mechanism can reduce the operating cost by 16.29% while reducing carbon emissions by 15.96%. The sensitivity analysis in this paper shows that when the carbon price increases by 50%, the annual net carbon reduction increases by approximately 3.4%. The difference in numerical magnitude mainly stems from the different carbon response channels at the planning level, but both confirm the positive incentive effect of carbon pricing on the selection of low-carbon technologies. A reasonable carbon pricing mechanism could obtain greater environmental benefits at a smaller economic cost, providing a quantitative basis for introducing the carbon market to rural areas. Equipment degradation, especially battery aging, had a prominent impact on economic performance. When the annual capacity retention rate of the battery dropped from 95% to 90%, the annualized cost increased by 7.0% and the carbon reduction decreased by 2.0%. This suggested that in actual engineering, technologies with long cycle life for energy storage should be prioritized, or battery replacement strategies should be embedded in the planning model. The impact of load prediction deviation was asymmetric. A 10% increase in load led to a 5.3% increase in cost and a 4.1% decrease in carbon reduction, while a 10% decrease in load only resulted in a 3.5% decrease in cost and a 3.6% increase in carbon reduction. The system is more sensitive to unexpected high loads, and an appropriate capacity margin should be reserved during deployment, and short-term load forecasting should be strengthened.

6 Conclusion

The research focused on the dynamic planning problem of rural integrated energy systems under the background of economic development, proposing a planning framework that deeply integrates stage division and MOIPOA. The effectiveness of this framework was verified through practical cases. The results showed that MOIPOA, with Sobol sequence initialization and ADF mechanism, effectively overcame the defects of traditional NSGA-II and MOPSO algorithms, such as being prone to local optimization and uneven distribution of Pareto solutions, and demonstrated better convergence accuracy and solution diversity. The optimal solution of the algorithm had an annual total cost of 1485.6 million yuan, which was 2.5%–4.9% lower than the comparison algorithms; the annual net CER was 634.2 tons, increasing by 3.7%–7.0%; the comprehensive energy efficiency of the system reached 76.8%, and the Pareto distribution index was only 0.082. It achieved a synergistic optimization of economicity, low-carbon benefits, and energy efficiency. This framework provided a feasible decision-making tool for the coordinated promotion of rural energy low-carbon transformation and rural revitalization in China. The wind, solar, biomass multi-energy complementation and energy storage peak-valley arbitrage strategies could fully activate rural renewable resources and help implement the "dual carbon" strategy, narrow the energy development gap between urban and rural areas, and have important practical guiding value.

However, the social factors such as user demand response and community governance models in the model are still relatively simplified. In the future, it can be combined with rural energy behavior surveys and social network analysis. In terms of the algorithm, MOIPOA still has room for improvement in terms of calculation efficiency and stability when dealing with higher-dimensional and multi-period coupled planning problems. It can be explored to combine with distributed computing and deep learning methods. Finally, the case verification of this study is limited to a typical rural area in northern China, which has abundant solar resources and high winter heating demand. The generalization and robustness of the framework in different climate zones and different economic development stages have not been fully verified. Future research should select multiple rural areas with significant geographical, economic and resource differences for empirical comparison to comprehensively evaluate the adaptability of the framework in different scenarios.

Fundings

This paper is a phased research achievement of the 2026 Soft Science Research Project of Henan Province "Study on the Potential Risks and Resilient Governance of Large-scale Poverty Return in Rural Areas of Henan Province under the Background of Rural Revitalization" (No. 262400411197).

Conflict of Interest Statement

The author declare that he have no known competing financial interests or personal relationships that could have appeared to influence the work reported in this paper.

References

Chander, N., & Upendra Kumar, M. (2024). Enhanced pelican optimization algorithm with ensemble-based anomaly detection in industrial internet of things environment. *Cluster Computing*, 27(5), 6491-6509. https://doi.org/10.1007/s10586-024-04303-y

Chen, J., Mao, C., Liu, Z., Ma, C., Sha, G., Duan, Q., Fan, H., Qiu, S., & Wang, D. (2023). Stochastic planning of integrated energy system based on correlation scenario generation method via Copula function considering multiple uncertainties in renewable energy sources and demands. *IET Renewable Power Generation*, 17(12), 2978-2996. https://doi.org/10.1049/rpg2.12805

Chen, W., Cao, Q., Cao, B., & Jin, B. (2025). An innovative coverage optimization method for smart information monitoring in agricultural IoT using the multi-strategy Pelican optimization algorithm. *Scientific Reports*, 15(1), 1-20. https://doi.org/10.1038/s41598-025-95885-z

Dong, W., Lu, Z., He, L., Zhang, J., Ma, T., & Cao, X. (2023). Optimal expansion planning model for integrated energy system considering integrated demand response and bidirectional energy exchange. *CSEE Journal of Power and Energy Systems*, 9(4), 1449-1459. https://doi.org/10.17775/CSEEJPES.2021.09220

Fu, X., Wei, Z., Sun, H., & Zhang, Y. (2024). Agri-energy-environment synergy-based distributed energy planning in rural areas. *IEEE Transactions on Smart Grid*, 15(4), 3722-3738. https://doi.org/10.1109/TSG.2024.3364182

He, J., Xiong, C., Li, Z., Mei, R., Zhao, X., & Wu, H. (2025). Research on aerial radioactive hotspot detecting based on an improved pelican optimization algorithm. *Journal of Radioanalytical and Nuclear*

Chemistry, 334(6), 4159-4170. https://doi.org/10.1007/s10967-025-10176-1

Irshad, A. S., Ueda, S., Furukakoi, M., Zakir, M. N., Ludin, G. A., Elkholy, M. H., Yona, A., Elias, S., & Senjyu, T. (2024). Novel integration and optimization of reliable photovoltaic and biomass integrated system for rural electrification. *Energy Reports,* 11, 4924-4939. https://doi.org/10.1016/j.egyr.2024.04.057

Jabari, M., Ekinci, S., Izci, D., Bajaj, M., & Zaitsev, I. (2024). Efficient DC motor speed control using a novel multi-stage FOPD(1+PI) controller optimized by the Pelican optimization algorithm. *Scientific Reports*, 14(1), 1-25. https://doi.org/10.1038/s41598-024-73409-5

Kocaturk, A., Orkcu, H. H., & Altunkaynak, B. (2025). Parameter optimization in biclustering algorithms for large datasets using a combined approach of NSGA-II and TOPSIS. *International Journal of Data Science and Analytics*, 20(6), 5499-5516. https://doi.org/10.1007/s41060-025-00782-3

Liu, J., Bai, Y., & He, Y. (2025). Optimal allocation of distributed energy storage in active distribution network via hybrid teaching learning and multi-objective particle swarm optimization algorithm. *International Journal of Electrical Engineering and Education*, 62(2), 144-163. https://doi.org/10.1177/0020720920983695

Liu, P., Wu, Y., Sun, J., & Zhao, J. (2025). Coordinated optimization of control parameters for improving the stability of wind-PV hybrid power systems under improved pelican optimization algorithm. *Electrical Engineering,* 107(4), 5163-5186. https://doi.org/10.1007/s00202-024-02782-1

Liu, Z., Fu, J., Zhang, X., & Ji, Q. (2025). Higher-order moment risk spillovers between the carbon and energy markets under climate policy uncertainty. *Journal of Management Science and Engineering,* 11(1), 1-19. https://doi.org/10.1016/j.jmse.2025.11.001

Ma, G., Hu, S., Pang, N., & Zhou, Q. (2025). Strategy improved pelican algorithm optimization ELM for short-term electricity load forecasting. *Distributed Generation and Alternative Energy* Journal, 40(1), 85-108. https://doi.org/10.13052/dgaej2156-3306.4014

Mary, V. B., Narmadha, T. V., & William Christopher, I. (2025). Hybrid power generating system sources and load synchronization using adaptive-neural-fuzzy-inference-system and pelican optimization algorithm technique. *IETE Journal of Research*, 71(1), 259-271. https://doi.org/10.1080/03772063.2024.2404524

Mohan, Y., Yadav, R. K., & Manjul, M. (2025). EECRPOA: energy efficient clustered routing using pelican optimization algorithm in WSNs. *Wireless Networks*, 31(5), 3743-3769. https://doi.org/10.1007/s11276-025-03970-y

Mu, Y., Guo, H., Wu, Z., Jia, H., Jin, X., & Qi, Y. (2024). A two-layer low-carbon economic planning method for park-level integrated energy systems with carbon-energy synergistic hub. *Energy and Artificial Intelligence*, 18(4), 291-308. https://doi.org/10.1016/j.egyai.2024.100435

Nassar, S. M., Saleh, A. A., Eisa, A. A., Abdallah, E. M., & Nassar, I. A. (2025). Optimal planning of integrated nuclear-hybrid renewable energy systems for electrical distribution networks based on artificial intelligence. *Scientific Reports,* 15(1), 1-24. https://doi.org/10.1038/s41598-025-11049-z

Qin, M., Xu, Q., Liu, W., & Xu, Z. (2024). Low-carbon economic optimal operation strategy of rural multi-microgrids based on asymmetric Nash bargaining. *IET Generation, Transmission and Distribution,* 18(1), 24-38. https://doi.org/10.1049/gtd2.12959

Sakka, S. (2025). Optimizing biogas production from household waste: an economical approach to energy and environmental sustainability in rural areas. *Euro-Mediterranean Journal for Environmental Integration,* 10(4), 3205-3215. https://doi.org/10.1007/s41207-025-00769-3

Serat, Z., Fatemi, S. A. Z., & Shirzad, S. (2023). Design and economic analysis of on-grid solar rooftop PV system using PVsyst software. *Archives of Advanced Engineering Science*, 1(1), 63-76. https://doi.org/10.47852/bonviewAAES32021177

Shahrom, S. F., Aviso, K. B., Tan, R. R., Saleem, N. N., Ng, D. K. S., & Andiappan, V. (2023). Regional planning and optimization of renewable energy sources for improved rural electrification. *Process Integration and Optimization for Sustainability,* 7(4), 785-804. https://doi.org/10.1007/s41660-023-00323-0

Song, H. M., Wang, J. S., Hou, J. N., Wang, Y. C., Song, Y. W., & Qi, Y. L. (2025). Multi-strategy fusion pelican optimization algorithm and logic operation ensemble of transfer functions for high-dimensional feature selection problems. *International Journal of Machine Learning and Cybernetics,* 16(7), 4433-4470. https://doi.org/10.1007/s13042-024-02517-5

Wang, D., Li, H., Li, J., Yu, Y., & Zhao, Y. (2024). Optimal configuration of rural integrated energy storage systems considering multiple demand-side responses. *Journal of Nanoelectronics and Optoelectronics,* 19(11), 1186-1194. https://doi.org/10.1166/jno.2024.3681

Wang, M., Gao, M., Cao, H., Yan, Z., Taimoor, M., & Xu, J. (2026). Policy impact of national comprehensive pilot initiative for new-type urbanization on carbon emissions from rural energy consumption in China. *Environment, Development and Sustainability*, 28(3), 5823-5851. https://doi.org/10.1007/s10668-024-05206-z

Wang, Q., Zhang, X., Xu, Y., Yi, Z., & Xu, D. (2025). Planning of stationary-mobile integrated battery energy storage systems under severe convective weather. *IEEE Transactions on Sustainable Energy,* 16(2), 1253-1268. https://doi.org/10.1109/TSTE.2024.3513295

Wei, M., Chen, J., Qi, X., Chen, Y., Zhang, K., & Sun, Z. (2026). Hierarchical rolling scheduling of electric-hydrogen-ammonia integrated energy system with long- and short-term multi-timescale optimization. *IEEE Transactions on Industry Applications,* 62(4), 5609-5622. https://doi.org/10.1109/TIA.2025.3644990

Wu, C. (2025). Carbon emission evaluation and low carbon economy optimization scheduling of rural integrated energy system based on LCA method. *IEEE Access*, 13, 17182-17194. https://doi.org/10.1109/ACCESS.2025.3533099

Xu, Y., Mu, Y., Jia, H., Zhang, J., Jin, X., & Wu, Z. (2026). Model predictive control method for an integrated community energy system based on a GRU-driven dynamic energy hub. *IEEE Transactions on Sustainable Energy,* 17(3), 2460-2471. https://doi.org/10.1109/TSTE.2026.3651984

Xu, Y., Sang, B., & Zhang, Y. (2025). Application of an improved pelican optimization algorithm based on comprehensive strategy in PV parameter identification. *Scientific Reports,* 15(1), 1-25. https://doi.org/10.1038/s41598-025-04396-4

Yi, L., Cheng, S., Wang, Y., Ma, H., Luo, B., & Hu, Y. (2024). A multi-objective pelican optimization algorithm for dynamic reconfiguration of multi-type rural rooftop PV array. *Journal of Intelligent and Fuzzy Systems,* 47(5-6), 393-409. https://doi.org/10.3233/JIFS-236528

Yu, Y. S., Chen, C., Wang, Y., Yu, H., Pei, C., Ren, J., Yang, L., & Lin, Z. (2025). Station-network cooperative optimization planning of urban integrated energy system considering heat storage capacity of heat network. *IEEE Transactions on Sustainable* Energy, 16(3), 1956-1976. https://doi.org/10.1109/TSTE.2025.3542549

Zhang, C., Qi, Y., Cao, X., & Zhang, Y. (2026). Low-carbon economic dispatch of an integrated energy system with multi-device coupling under ladder-type carbon trading. *Energy Engineering,* 123(2), 294-313. https://doi.org/10.32604/ee.2025.069878

Zhang, J., Chang, X., Xue, Y., Bai, X., Li, Z., Wang, P., & Sun, H. (2025). Optimal planning for electricity-gas-hydrogen integrated energy systems considering intertemporal long-term hydrogen storage and multiple uncertainties. *IEEE Transactions on Power Systems,* 40(6), 4660-4674. https://doi.org/10.1109/TPWRS.2025.3577703

Zhang, X., Ding, C., Liang, G., Yang, P., & Wang, X. (2024). Research on integrated energy system planning based on the correlation between wind power and photovoltaic output. *IET Renewable Power Generation,* 18(11), 1771-1782. https://doi.org/10.1049/rpg2.13054